Proceedings of FEDSM2005
2005 ASME Fluids Engineering Division Summer Meeting and Exhibition
June 19-23, 2005, Houston, TX, USA

FEDSM2005-77359

USING X-RAYS FOR MULTIPHASE FLOW VISUALIZATION

Theodore J. Heindel[†] and Jeremy L. Hubers
Department of Mechanical Engineering
Iowa State University
Ames, IA 50011-2161
USA

Terrence C. Jensen, Joseph N. Gray, and Alexander C. Striegel
Center for Nondestructive Evaluation
Iowa State University
Ames, IA 50011-3042
USA

ABSTRACT

Gas-liquid, gas-solid, liquid-solid, and gas-liquid-solid multiphase flows are difficult to visualize, characterize, and quantify because the systems are typically opaque. Invasive or noninvasive measurement methods are typically used for determining internal flow and transport characteristics of these complex flows. The difficulty with invasive methods is that they can alter the internal flow of a multiphase system causing interference with realistic process measurements. X-ray imaging provides one family of noninvasive measurement techniques used extensively for product testing and evaluation of static objects with complex structures. These techniques have been extended to visualize dynamic systems, such as those which characterize multiphase flows.

This paper will describe a new X-ray flow visualization facility for large-scale multiphase flows. X-ray radiography and X-ray computed tomography of static and dynamic systems will be used to demonstrate system capabilities. Radiographic images will show bread dough rising, objects falling in a liquid, large bubbles rising in a 32 cm ID column of water, and operation of a 32 cm ID bubble column. X-ray computed tomography of a large static object will demonstrate visualization capabilities. X-ray computed tomography of a multiphase flow in a 32 cm bubble column will show local time-averaged gas holdup values for various operating conditions. Finally, challenges associated with X-ray stereographic imaging to capture time-resolved dynamic events will be outlined.

INTRODUCTION

Multiphase flows are found in many process industries including fuel production, commodity and specialty chemical production, mineral processing, pulp and paper production, wastewater treatment, food processing, and biological organism and pharmaceutical production [1]. Multiphase flow hydrodynamics and operations are quite complex, and while many industries utilize multiphase flows, a better understanding of the transport and hydrodynamic characteristics are needed for process improvement and optimization. In order to identify internal flow characteristics of multiphase flows, one can use either invasive measurement techniques or noninvasive methods. All invasive methods can potentially alter the internal flow, whereas noninvasive methods eliminate this concern.

Noninvasive measurement techniques for multiphase flows are being developed by several research groups in an attempt to provide high quality quantitative data of various flow characteristics. It has been repeatedly stressed that such data are necessary to improve and validate multiphase flow models [1-3]. Noninvasive measurement techniques have been reviewed in the literature [4-6]; they include electrical impedance tomography (EIT) [7], electrical capacitance tomography (ECT) [8-11], ultrasonic computed tomography (UCT) [12-14], gamma densitometry tomography (GDT) [15-17], and X-ray computed tomography (XCT) [18-21]. Many of these techniques offer trade-offs when implemented [4, 6]. For

[†] Corresponding author: theindel@iastate.edu, 515-295-0057

example, ECT is very fast but the spatial resolution is poor and the results are sensitive to the reconstruction algorithm, UCT has average spatial and temporal resolution but is better suited for low solid and gas holdup systems, and XCT has excellent spatial resolution but poor temporal resolution – it is best for providing time-average phase distributions. Other groups have developed individual particle tracking methods using radioactive emitting tracer particles [22] or X-ray absorbing particles [23-25]. Yet others have used radiographic [26] and fluoroscopic [27] imaging to view internal gas flow characteristics of slurry flows.

The objective of this paper is to describe the X-ray hardware, software, and facilities that allow for the study, characterization, and measurement of various multiphase flow characteristics in large vertical systems that have internal diameters of up to 32 cm and can be studied at several axial locations spanning nearly 4 m. In addition to typical digital X-ray radiography capabilities, the imaging system allows for X-ray computed tomography (i.e., CT scans) of multiphase flows in large vertical columns, providing time-averaged local phase distributions. Digital X-ray radiography and X-ray computed tomography of various systems will be demonstrated. The X-ray imaging system also includes a novel application of X-ray stereography and stereographic reconstructions to visualize time-resolved flow structures in three dimensions, and the implementation of this technique will be described.

NOMENCLATURE

C	fiber mass fraction
CT	computed tomography
ECT	electrical capacitance tomography
EIT	electrical impedance tomography
GDT	gamma densitometry tomography
U_g	superficial gas velocity
UCT	ultrasonic computed tomography
XCT	X-ray computed tomography

Symbols

ε_g	gas holdup
ϕ	volume fraction
μ	linear attenuation coefficient

Subscripts

g	gas
l	liquid
s	soid

X-RAY FLOW VISUALIZATION FACILITY

The Iowa State University X-ray flow visualization facility, referred to as the XFloViz facility, is schematically represented in Fig. 1. The facility includes a lead-lined room that is 3.7 m off the laboratory floor. The X-ray imaging system consists of two X-ray sources and two image intensifiers, offset 90° from each other. The X-ray sources and image intensifiers are mounted on a slewing ring (a donut-shaped gear) with a

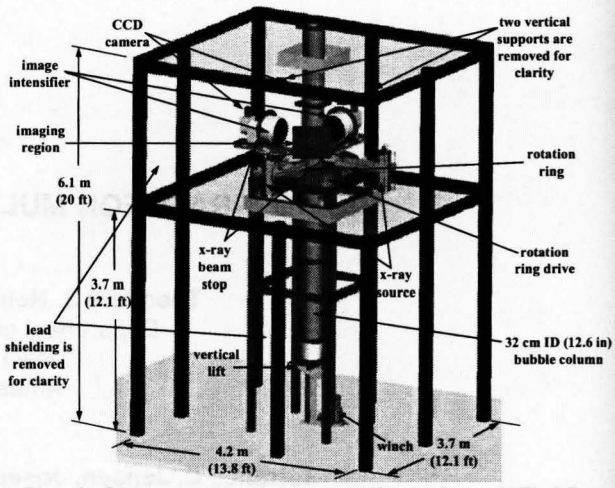

Fig. 1. Schematic representation of the XFloViz facility.

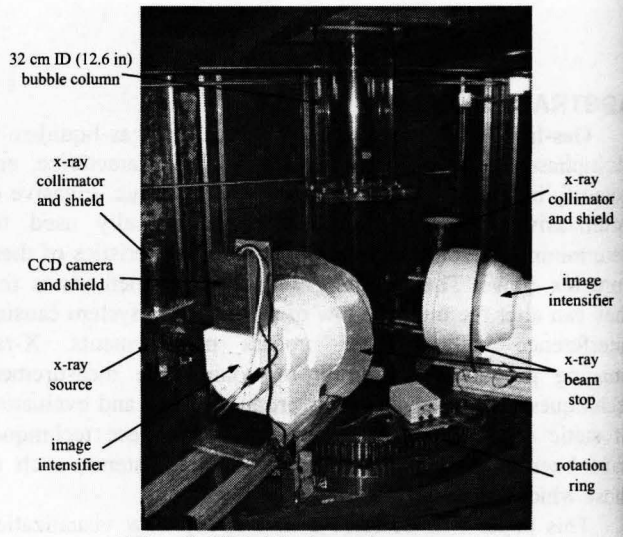

Fig. 2. XFloViz imaging room.

101.4 cm ID which allows complete rotation around the imaging region. Figure 2 shows the actual imaging facility with a 32.1 cm bubble column installed in the facility and two x-ray source/image intensifier pairs mounted on the rotation ring.

Two LORAD LPX200 portable X-ray tubes with beryllium windows and a 1.5 mm focal spot size provide the x-ray sources. The maximum power is 900 W with adjustable voltage (10-200 kV) and current (0.1-10.0 mA) capabilities. The windows provide a 60° horizontal and 40° vertical conical X-ray beam. A 1 mm copper filter has been added to the tube windows to suppress low energy radiation, and a 2.9 cm

diameter collimator is used to limit the beam to the diameter of the bubble column.

The image intensifiers are Precise Optics PS164X 40.6 cm diameter screen detectors with an output image diameter of 35.0 mm. The CCD cameras that read the image from each intensifier are DVC-1412 monochrome digital cameras with a pick up area of 8.98 mm × 6.71 mm. The pixel size is 6.45 μm × 6.45 μm, and the active pixels are 1388(H) × 1024(V). The cameras have binning capabilities of 1 × 1 at 10 frames/second (fps), 2 × 2 at 20 fps, 4 × 4 at 40 fps, and 8 × 8 at 60 fps. A 44 × 44 cm cesium-iodide scintillator screen coupled to a third CCD camera is being installed as an alternative to the image intensifiers. The third CCD camera is an Apogee Alta U9 system with a sensor array of 3072(H) × 2048(V) pixels, with a pixel size of 9 μm × 9 μm. It has a thermoelectric cooler to enable low-noise, long exposures, and options to digitize signals at either 12 or 16 bits. This third camera system is not well suited for real-time imaging, but will supply superior images for time-averaged CT reconstruction.

The slewing ring is driven by a Parker stepper motor and controlled by the data acquisition computer. X-ray images are taken every 1° around a 360° path to produce a time-averaged local phase distribution CT image. A single source/detector pair is used for the CT data. The dual source/detector pairs are used for X-ray stereographic imaging. The X-ray sources can be finely adjusted vertically in order to center the beam on the detectors. The image intensifiers can slide in a radial direction in order to move the intensifiers close to the object of interest, thereby changing the magnification of the object in the image.

While the rotation ring is set in place vertically, the multiphase flow of choice (or other imaging object) rests on a platform connected to a 910 kg (2000 lb) vertical lift. The lift can travel over 2.75 m, and with a platform extension, the imaging region in the vertical direction can traverse over 4 m.

Image acquisition for the XFloViz system is controlled by a personal computer with 4 GB of RAM and custom software developed by the Center for Nondestructive Evaluation (CNDE) at Iowa State University. The software was designed and written to integrate motion control and data acquisition for digital X-ray radiography, X-ray computed tomography, and X-ray stereography data collection [28]. The CT reconstruction algorithm is filtered back-projection. Due to the hardware used, a variety of image corrections are applied to produce the best image. These image "flaws" include the warping effects created by the image intensifier, individual pixel nonuniformity, and beam hardening. To account for these effects, algorithms were created to unwarp the image, normalize the pixel response, and correct for beam hardening [28]. Image reconstruction is completed on a 64-node LINUX cluster available at CNDE. Custom visualization software is also provided by CNDE and can run on most personal computers.

SYSTEM DEMONSTRATIONS

Several radiographic and CT images have been acquired to demonstrate capabilities of the XFloViz facility. Some of these demonstrations are provided below. Although not all the images are of multiphase flows, they all quantify system capabilities.

X-ray Radiography

X-ray radiography is the process of recording a two-dimensional image of a three-dimensional object by recording the X-ray attenuation through the object. Digital radiography has seen a tremendous increase in popularity in the last five years due largely to improved performance of CCD sensors and computer power capable of processing the large data set generated in digital radiography. Major advantages of digital radiography over more traditional film radiography are the speed with which images can be acquired and the flexibility in manipulating and storing images.

The XFloViz facility is capable of producing radiographs at a variety of temporal and spatial resolutions, depending on the detector system and the CCD camera frame rate and binning options. The resulting images can be assembled into a movie to view the object in motion. Images below are selected frames from the image acquisition process.

Bread Dough Rising: The movement of a phase front is important to ablation casting and fluid movement in porous material or fibrous mats. The rising of bread dough can be used to simulate the movement of a phase front. Figure 3 reveals eight frames of a compilation of radiographs showing bread rising. The imaging was completed using one x-ray source/detector combination set at 81 kV and 0.6 mA. The CCD camera was set at 2 × 2 binning (20 fps) and each radiograph is an integration of 30 frames to increase contrast sensitivity. Radiographs were taken every 5 minutes.

In addition to recording the growth of the dough surface, the formation and collapse of gas bubbles can also be observed. The development of gas bubbles inside the rising dough can also be tracked, although they are difficult to view with limited gray scale resolution.

The time length shown in Fig. 3 (7 hours) is atypical for most bread rising. It is assumed that the x-ray radiation restricts the yeast activity in the process, thus increasing the time for the dough to rise a reasonable amount.

Ball Settling in Water: X-ray radiographic images of a rubber ball falling through a water-filled column were taken at 4 × 4 binning, which allowed a frame rate of 40 fps. Both X-ray source/detector systems recorded the settling ball, with simultaneous image acquisition by each CCD camera. The X-ray power setting for each source was 141 kV and 1.0 mA. The rubber ball was 5.08 cm (2.0") in diameter. An eyebolt was inserted into the ball in order to tie the end of the eyebolt to a retrieval line. This allowed the ball to be dropped through the water-filled column and then pulled back up again without difficulty. The density of the rubber ball and the eyebolt was greater than water, thus allowing a contrast in the X-ray image to distinguish between the water and the rubber ball and

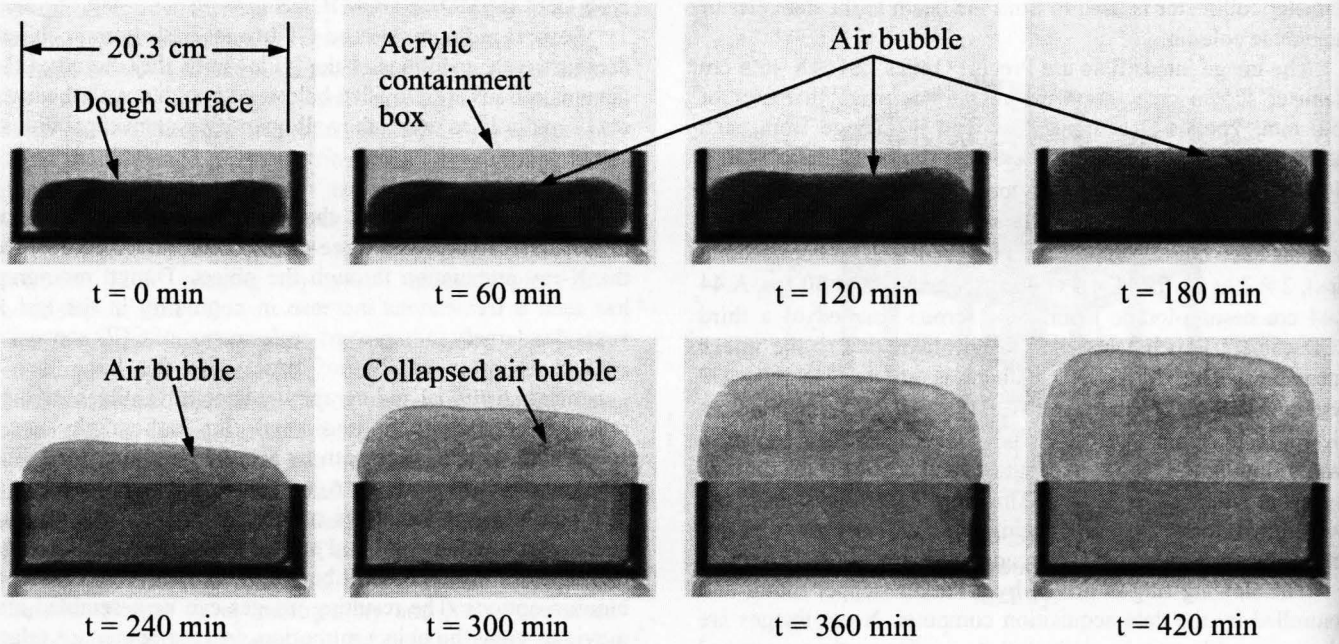

Fig. 3. Radiographs of rising bread dough.

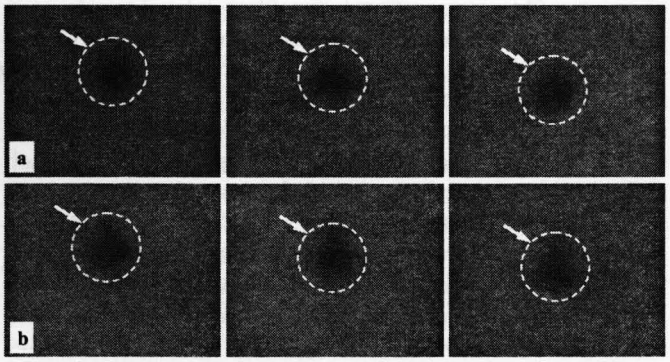

Fig. 4. Consecutive radiographic images of a rubber ball falling through a water-filled column using (a) camera 1 and (b) camera 2.

eyebolt. The terminal settling velocity of the ball was estimated through image analysis, theoretically calculations (with a range of drag coefficients), and timed analysis, where the settling ball was visually observed between two column sections and then timed with a stop watch [29].

Figure 4 shows three images from both cameras corresponding to consecutive images of the ball dropping through the column. These images have been enhanced in order to highlight the ball by dividing the ball drop frame by an average of 5 empty background frames and then applying an FFT filter to smooth out pixel noise. The approximate location of the ball in each image has been highlighted by an arrow and dashed circle. Note the circle does not imply the actual ball surface but the region in which the ball is located. Also, ball location is easier to identify in the visualization software, which can output actual linear attenuation values, than in the images shown in Fig. 4, which shows limited gray scale variations. However, determining the top and the bottom of the ball was still difficult and this provided the most error in the settling velocity calculations. For example, the average error from calculating the diameter of the ball in each image was ~5.4%; this corresponds to an error range in the settling velocity of almost 12 cm/s. Several frames were analyzed from both cameras from three trial runs to determine the ball settling velocity. Table 1 summarizes the results and compares them to theoretical calculations and timed ball drop trials, with the uncertainty assuming a 95% confidence level [29].

Table 1. Ball settling velocity.

Method	Settling Velocity (cm/s)
X-ray Analysis	49.5 ± 1.8
Theoretical	46.1 ± 0.49
Timed	46.0 ± 0.70

Large Bubble Rising: A 32 cm bubble column described elsewhere [30] was used to visualize a large bubble rising through a water-filled column. The bubble was generated by running the bubble column at a high superficial gas velocity (~15 cm/s) and then closing a ball value in the air line to stop the gas flow. After all the air bubbles ascended the column, the ball valve was abruptly opened to send a surge of air through the column. A vapor layer quickly formed on the bottom of the column and rose. Wall friction caused the shape of this air layer

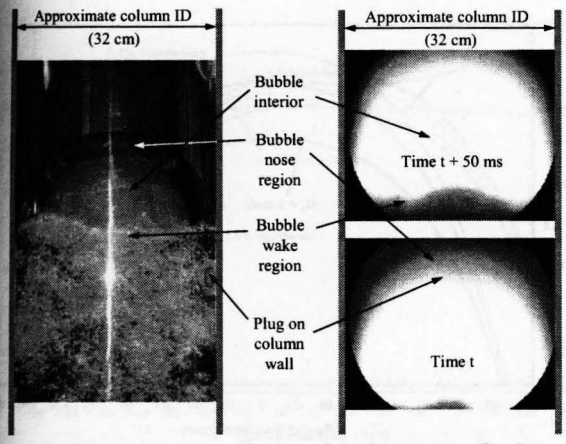

Fig. 5. Digital and radiographic images of a large bubble rising in a 32 cm column of water.

to form a bullet-nose bubble. Many small bubbles were entrained in the wake of the large bubble as it rose up the column. Figure 5 displays a digital picture of one large bubble rising up the column at an approximate location of 290 cm from the column aerator (~9 column diameters). This picture was taken with a handheld digital camera.

Radiographic images of similar large bubbles at a location of ~9 column diameters from the column floor were recorded at an X-ray power level of 141 kV and 1.0 mA and camera settings of 2 × 2 binning (20 fps). Some images were acquired with a single source/detector and some were recorded using both source/detector pairs. Figure 5 also shows 2 sequential images, separated by 50 ms, taken from one image intensifier. The large circular region that fills the majority of each image represents the image intensifier active area. The dark regions beyond this circular region are active pixel elements in the CCD camera, but do not record any image information.

Hubers [29] estimated the rise velocity of several different large bubbles rising through the 32 cm bubble column using visual observations and a stop watch and image analysis of radiographic images. The timed rise velocity using a stop watch was 67.3 ± 1.1 cm/s; the X-ray images revealed a rise velocity of 67.7 ± 5.3 cm/s. The larger error with the image analysis is attributed to the difficulty in identifying the air-water interface in the radiographs.

Bubble Column Operation: Radiographic imaging of the 32 cm ID bubble column in operation was also completed at an X-ray power setting of 141 kV and 1.0 mA. Figure 6 shows two sequential images of the gas flow in an air-water-cellulose fiber suspension where the cellulose fiber mass fraction is 1% and the superficial gas velocity is 3 cm/s. Assembling the radiographic images into a video reveals bubbles trapped in a recirculation cell near the column wall and large bubbles rising through the center of the column.

X-ray Computed Tomography

X-ray computed tomography (CT) generates a two-dimensional cross-sectional image of an object showing internal details. An X-ray source illuminates the object of interest and projects the resultant X-ray intensity onto an imaging device. Projections from each orientation are collected and reconstructed with standard algorithms [31, 32], generating an image of the object cross-section. Because an X-ray cone beam is used in the XFloViz facility, multiple slices can be acquired simultaneously by considering different rows of the CCD camera, and the resulting data can be reconstructed to provide three-dimensional CT images of the time-averaged phase distribution.

Loaf of Bread: Figure 7 shows a CT image of a loaf of bread. Although this is not a multiphase flow, it does show capabilities of the CT system and imaging software. This image was acquired in a single CT scan using 2 × 2 binning, 1° step in rotation, 30 integrated frames at each step, and a power setting of 77 kV and 0.5 mA. Because the source produces a cone beam, and the image intensifiers captures the X-ray attenuation information in a circular region, CT slices at different vertical locations can be produced from a single scan. These slices are stacked together to form a three-dimensional image. The image in Fig. 7 was produced by stacking together 250 CT slices, all of which were acquired during the same CT scan.

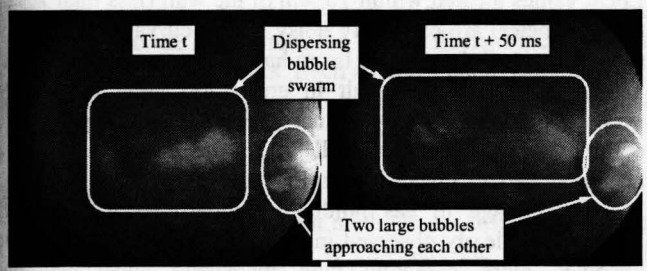

Fig. 6. Two sequential images of air rising through a 1% by weight cellulose fiber suspension.

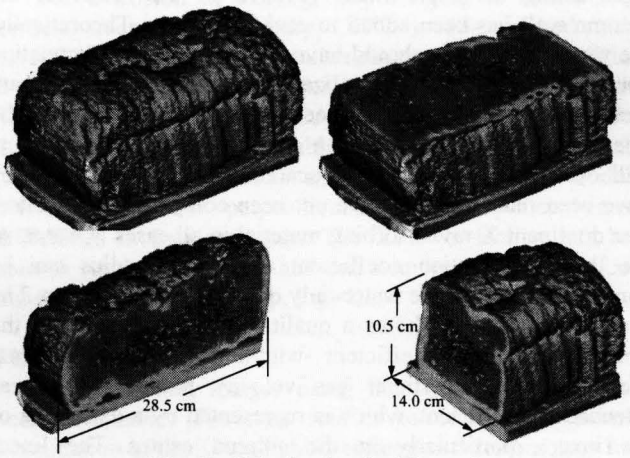

Fig. 7. CT of a loaf of bread.

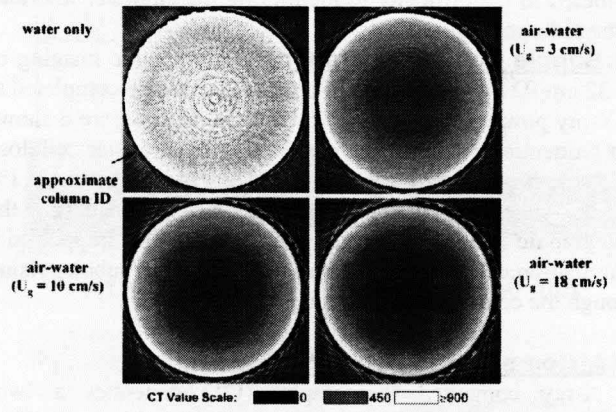

Fig. 8. CT images of an air-water system in a 32 cm ID bubble column [33].

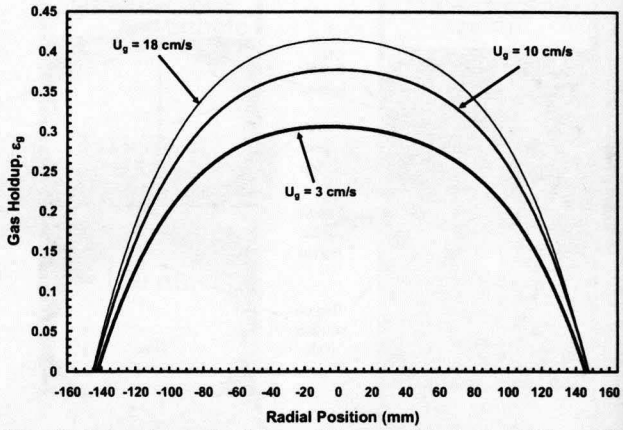

Fig. 9. Local gas holdup along a single ray through the column center in an air-water system.

This image shows the relative size of the imaging region that can be captured in a single CT scan – about the size of a loaf of bread. Also, the custom visualization software allows for filtering to make certain linear attenuation coefficient values and/or regions transparent. This ability is used to produce the sectioned views in Fig. 7 where internal features are observed.

32 cm ID Bubble Column: Time averaged local gas holdup in a bubble column can be determined using CT imaging; this was accomplished by acquiring CT images of the 32 cm bubble column at superficial gas velocities of U_g = 3, 10, and 18 cm/s. Air-water systems and air-water-cellulose fiber systems at fiber mass fractions of 0.1% and 1% have been imaged. These images were taken at a fixed column height of 290 cm from the aeration plate. A single source/detector pair was rotated 360° at 1° increments and an X-ray power of 141 kV and 1.0 mA was utilized. Linear pixel normalization and unwarping were applied to all projection images, and the CT scans have been corrected for beam hardening effects [28, 29].

Figure 8 shows a single CT slice of the air-water system at different superficial gas velocities [33]. A dashed line representing the approximate location of the inside of the column wall has been added to each CT image. Theoretically, the water only image should have a constant linear attenuation coefficient, so pixel normalization, unwarping, and beam hardening corrections have been applied to reconstruct the image as close as possible to a constant value. Ring artifacts will occur in third-generation scanning [34], and while they have been reduced, they have not been completely eliminated. The dominant X-ray absorbing material in all cases is water, so the linear attenuation coefficient at a given radius can be compared to that of the water-only data at the same radius. The gray scale variation shows a qualitative representation of the linear attenuation coefficient within the bubble column. Increasing the superficial gas velocity reduces the linear attenuation coefficient, which is represented by a darkening of the image, particularly in the column center. The linear attenuation coefficient correlates inversely with gas holdup; hence, Fig. 8 represents an increase in local gas holdup as superficial gas velocity increases, which is expected.

Local gas holdup (ε_g) at each pixel location can be derived from the CT images using [28]

$$\varepsilon_g = \frac{\dfrac{\mu}{\mu_l\phi_l + \mu_s\phi_s} - 1}{\dfrac{\mu_g}{\mu_l\phi_l + \mu_s\phi_s} - 1} \qquad (1)$$

where μ represents the linear attenuation coefficient and subscripts g and l represent air only and liquid only CT data sets. The subscript s corresponds to the solid phase and ϕ corresponds to the volume fraction in the liquid-solid slurry (i.e., when no gas is present). The term that combines the liquid and solid phases corresponds to the linear attenuation coefficients generated by a CT scan of a homogeneously mixed water-solid slurry. For the fiber suspensions used here, the liquid-solid term can be assumed to be approximately equal to that of water (homogeneously mixed). The local gas holdup variation shown in Fig. 9 corresponds to that position on a horizontal line drawn through the images in Fig. 8 that is coincident with the column center. Fourth-order curve fits are used to smooth the CT noise to determine local linear attenuation values. These values are then used in Eq. (1) to determine local gas holdup as a function of radius (Fig. 9). Local values located within 10 mm of the wall (less than 7% of total diameter) are extremely noisy due to curvature effects of the column and the applied beam hardening correction. Hence, values in this region result in errors too large to provide accurate gas holdup values. Since average gas holdup near the column wall is generally small [7, 35, 36], these values have been assigned a value of zero in Fig. 9.

The change in gas holdup as superficial gas velocity increases is clearly observed in Fig. 9. The gas holdup profile becomes more parabolic with increasing superficial gas velocity; this result has been observed by others [7, 35, 36].

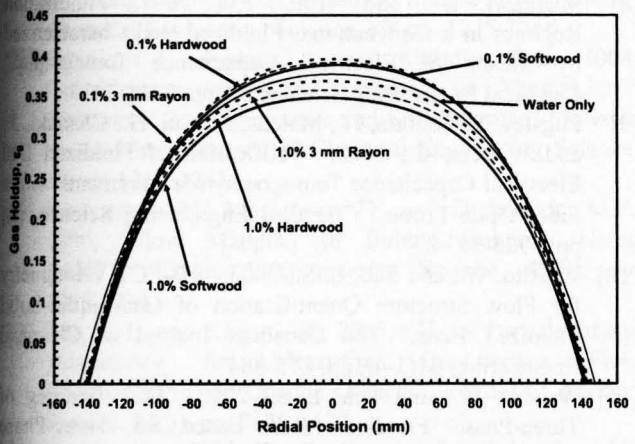

Fig. 10. Local gas holdup vs. radial position at U_g = 10 cm/s for air-water-fiber slurries of varying fiber types

Time-averaged local gas holdup values have also been obtained using air-water-fiber suspensions in the 32 cm bubble column. Hardwood and softwood cellulose fibers and 3 mm long Rayon fibers were used at mass fractions of C = 0.1% and 1% (Fig. 10). When C = 0.1% fiber is added the column, the local gas holdup increases above that of the air-water system. This has been attributed to severe backmixing and fibers preventing small bubbles from interacting with other bubbles. When a small mass fraction of fiber is present, they act as a separating medium between small bubbles and retard small bubble-bubble interaction [33]. This produces a slight increase in gas holdup when the fiber mass fraction is 0.1% for all fiber types.

When 1.0% fiber is added to the system, the effective slurry viscosity is much higher than that of water and larger bubbles are needed to break through the fiber network. These large bubbles have a shorter residence time in the system, producing a lower gas holdup at all radial positions when compared to the air-water system [33].

The above local effects are observed with all three fiber types used in this study. Among different fiber types, Rayon produces a higher local gas holdup than cellulose (natural) fibers. This is attributed to surface coatings that are applied to the Rayon fibers during manufacturing. Although these systems are vigorously washed before use [30] and no change in surface tension is observed, a small amount of surface active agents may leach into the water from the Rayon fibers which will act as bubble surface stabilizers. Even a trace amount can influence gas holdup and this is best captured by the local measurements recorded in Fig. 10.

X-ray Stereography

Stereographic measurement methods use information from two 2-dimensional projections to calculate the 3-dimensional location of features in an object [37]. This can be accomplished by analyzing two images of an object which are taken at

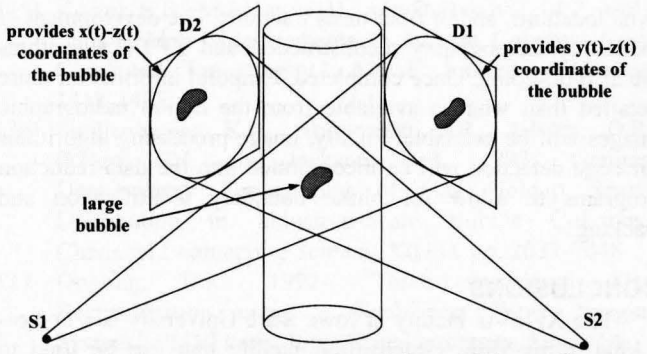

Fig. 11. X-ray stereography; S1 and S2 are X-ray sources and D1 and D2 are X-ray image intensifiers.

different positions either due to a rotation or translation of the sample. With the two source/detector pairs in the XFloViz facility, and using appropriate software controls for the two CCD cameras, two images can be acquired simultaneously. As long as the point of interest is identifiable in both images, its corresponding three dimensional coordinate can be determined. Although not required, accuracy of the coordinate determination can be increased through the use of markers at known locations in the object of interest. Doering [37] was able to measure points in several small static samples with an accuracy of 0.1 mm. Jensen and Gray [38] utilized this technique for visualizing molten aluminum flow in lost foam castings.

Hence, stereographic imaging can produce a three dimensional map of a feature of interest as a function of time. With successive continuous images, the three dimensional location of a multiphase flow feature, such as a bubble, can be determined as a function of time (Fig. 11). Characteristics such as object rise and settling velocity or breakup and coalescence rate, could then be determined from these data. This provides a means for three dimensional X-ray flow visualization of dynamic characteristics, at a temporal resolution comparable to the frame rate of the CCD cameras.

An extension of stereography imaging is called X-ray particle tracking velocimetry (XPTV); this method tracks several objects (particles) simultaneously as a function of time. By tracking neutrally buoyant X-ray absorbing particles, Seeger et al. [24, 25] were able to record the three-dimensional liquid velocity field in the bubble column. They were not able to synchronize their CCD cameras, so there was a delay between the two perpendicular images, which caused difficulties in data reduction. The XFloViz facility has been able to resolve this issue and can acquire two perpendicular images simultaneously (e.g., Fig. 4).

FUTURE WORK

Demonstration images using the XFloViz facility have been completed. The next step is to complete a detailed examination of the 32 cm bubble column to determine any local variations in gas holdup at different superficial gas velocities,